



**Manchester
Metropolitan
University**

Dwivedi, Pooja and Maheshwari, Sachin and Abidi, Mustufa Haider and Sid-diquee, Arshad Noor and Haider, Julfikar and Alkhalefah, Hisham (2022) Towards devising pilot experiments to establish parameter window for FSP of aluminum alloys. *Advances in Mechanical Engineering*. ISSN 1687-8132 (In Press)

Downloaded from: <https://e-space.mmu.ac.uk/629834/>

Version: Accepted Version

Publisher: SAGE Publications

Please cite the published version

<https://e-space.mmu.ac.uk>

Towards Devising Pilot Experiments to Establish Parameter Window for FSP of Aluminum Alloys

Pooja Dwivedi¹, Sachin Maheshwari¹, Mustufa Haider Abidi^{2*}, Arshad Noor Siddiquee³, Julfikar Haider⁴, Hisham Alkhalefah²

¹ Division of Manufacturing Processes and Automation Engineering, Netaji Subhas Institute of Technology, New Delhi-110078, India;

² Advanced Manufacturing Institute, King Saud University, Riyadh-11421, Saudi Arabia;

³ Department of Mechanical Engineering, Jamia Millia Islamia, New Delhi-110025, India;

⁴ School of Computing Engineering and Information Sciences, Ellison Building, Northumbria University, Newcastle Upon Tyne, NE1 8ST, United Kingdom;

Corresponding authors: mabidi@ksu.edu.sa

Abstract

One of the major challenges encountered during friction stir processing (FSP) is the establishment of a process parameter window in order to achieve processed surfaces with an acceptable quality as it is an exhaustive task that involves enormous resources, time and efforts. Sometimes this task is so difficult that the trial may run into futility. This work belongs to a theme of FSP that is not much reported in the literature. This is a maiden work to lay a roadmap for the FSP parameter range in a quick and effective manner. The present study results from first-hand experiments performed to produce surface composites on AA6063 alloy using a mixture of SiC+Fe+Mn+Sn as reinforcement in such a manner that a novice professional can pan out ways to identify and classify irregularities/defects, associate them with the causes and obtain feasible parameter window. In this work, a methodology for identification and selection of optimum tool speed (rpm), processing speed and plunge depth has been demonstrated. The parameter window was established by analysing main surface irregularities associated with the parameters and taking corrective modification to eventually arrive at the feasible range. The established range was validated through an experiment performed with the parameters lying within the established window. The validation was supported with microstructural characterization, micro-hardness measurement, thermal analysis, corrosion analysis and the comprehensive analysis presented in this work has been done with the help of the image processing technique. Results show that grain refinement and homogeneous distribution of reinforcement present in the stir zone developed during FSP at the appropriate process parameters. Furthermore, grain refinement enhances the hardness by 28.29% and the corrosion resistance by 13.6%. The highest temperature i.e. 423.25°C is achieved on the advancing side of the processed zone.

Keywords: Friction Stir Processing; AA6063 alloy, surface composite, Parameter Range Identification; Defect Irregularity and Elimination.

1. Introduction

Friction Stir Processing (FSP) is a recent and versatile solid-state technique that was initially developed for microstructural modifications and mechanical properties enhancement through grain refinement and dynamic recrystallization. Of late, it has evolved as a generic material processing technology. It utilizes a rotating cylindrical tool with a shoulder and a pin, which plunges into the base metal (BM) surface and subsequently traverses in a predefined direction. The frictional heat input between the tool and BM and associated plasticization softens the material [1]. The term softening temperature is often associated with the temperature of the material at which it undergoes processing and it is close to its recrystallization temperature. The material flow during FSP generates a spatial movement and results in intimate mixing through stirring action. Severe plastic deformation is achieved at softening temperature during stirring which produces ultra-fine grains and enhances the strength and toughness due to dynamic recrystallization (DRX) [2].

Thus, FSP is highly useful in producing composites by embedding and dispersing reinforcement particles into the substrate. While the process is so generic and promising, it possesses the challenges of its own kind such as the very beginning of the processing may be extremely difficult if not impossible [3]. The success of the acceptable processed zone closely depends on several factors including tool design and fixed and variable process parameters. The process parameters such as tool geometry,

plate dimension also exert significant influence on the microstructure evolution and the processed regions of acceptable quality [4].

Entire material property evolution during FSP closely depends on the adequacy of material flow which also affects the state of defects in the processed zone. The presence of FSP related defects makes the entire processing futile as a defect per se weakens the rest of the processed zone howsoever strong it may be. An ineffective material flow during the FSP is the origin of the defect formation such as wormhole, tunnel defect, voids [5]. Thus, identification, classification and characterization become very important for the alleviation of defects. Image processing can be effectively utilized in the defect analysis of materials processed via different routes. Through this technique, the image quality is controlled to extract the exact details of specific defects. This technique plays a critical role in the welding industry for seam tracking and in welding research for process monitoring [6]. Several image processing techniques such as image pyramid and image reconstruction have been used for the defect analysis in Friction Stir Welding (FSW) [7].

A structured way for identification and classification of irregularities and elimination of associated causes can produce acceptable processed regions. Such irregularities are the serious obstruction encountered during trials and pilot studies. To gauge the importance of the trial experiment, several interactions with the researchers and scholars were carried out. The interactions prompted that there is little to guide for an experiment during the trial phase. It was noticed that if the analysis of irregularities is not accurately carried out, then the trial experiment may become very lengthy and time- and resource-consuming. It is well established that the experimental investigation requires a step-by-step approach from identifying parameters to analyzing results [8]. In a typical research, a procedure depicted in Fig 1 is commonly followed.

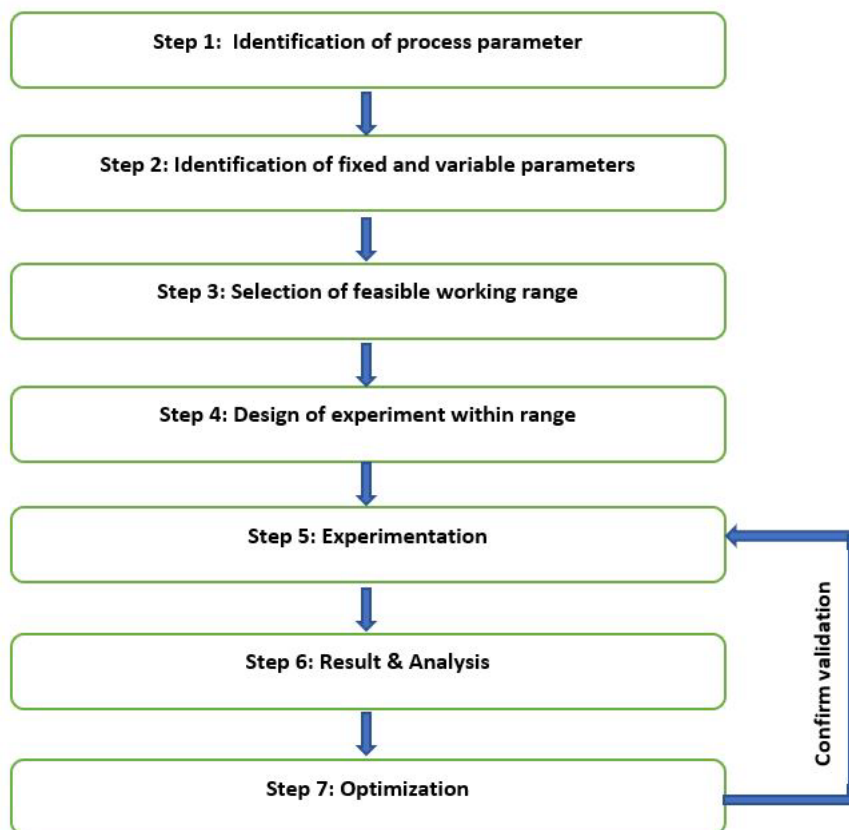


Fig. 1 Flow chart of experimental investigation of FSP/FSW procedure

For Steps 1 to 3, one has to mostly rely on handbook knowledge and expert opinion as the literature does not provide due support for a range identification. Furthermore, maximum efforts in terms of material, man and machine hours are invested in the trial experiments and pilot studies (Step 3). This task is exhaustive and costly in the absence of a robust simulation platform with a dedicated module for this process. Once the range is established through pilot/trial experiments, the optimization is performed through the design of experiments which is systematic and simple. For validation, experimentation is performed within the parameter range. Therefore, when the range is identified correctly, experimentation is not much of a challenge.

Whereas, ample literature is available on the surface defects, the irregularities which remain a major issue are not reported frequently. The available literature is focused more on defects like surface grooves, flash, tunnel defect, kissing bond, hooking and joint line remnant which mainly occur during FSW [5, 9-11], whereas the focus on defects which are typical to the FSP

and especially those which are encountered during trials is scant. During the initial phase, the selection of fixed parameters (such as slot size, pin offset, pin length & diameter, shape and profile of pin, shoulder diameter, tilt angle etc.) are very important and crucial for making a defect-free acceptable processed zone.

Kim et al. studied the surface defects namely flash and groove occurred during FSW in which flash was ejected due to metal softening at high heat input and groove like defect was caused by insufficient heat input owing to higher welding speed and lower rotational speed [9]. Kah et al. reported that tool pin height and plunge depth are closely related to the plate thickness as an impromptu selection of these process parameters can cause defects [12]. A very high rotational speed delivers excessive heat input which results in a very high softening adjacent to the shoulder and the excessively softened material is expelled in large amounts by forming flash. The excessively softened material finds it easy to get squeezed out under high shoulder pressure rather than being forged behind and getting consolidated [13]. Insufficient plunge depth causes groove defect at the advancing side of the plate. Wormholes and tunnel defects generally appear in the advancing side (AS) and are mainly caused by poor heat input and inefficient material flow [14]. The kissing bond and joint line remnant defects occur due to low heat input caused by low rotating and high traversing speeds [15]. In almost all the reported works, the defects were analysed through macro and microstructural analysis which requires extensive surface preparations and technical skills [16].

Defect analysis in the FSP/FSW could be performed by several non-destructive methods like immersion ultrasonic and phase array ultrasonic techniques, X-ray radiography thermography, eddy current testing, synchrotron radiation etc. [17]. These techniques are typically suitable for the sub-surface defects. Therefore, surface irregularities especially, those formed during the initial phases of FSP, are inutile. Images processing technique becomes very useful and simple particularly for the surface defects. The image processing technique is non-destructive, and analysis can be done in "as is" condition. This investigation has attempted to establish a roadmap on how irregularities and defects of processed material could be perceived towards taking corrective measures to alleviate the irregularities and producing an acceptable experiment regime. For common researchers/professionals it is a very tedious, challenging task to get the first successful FSP pass; leave aside a feasible working range of parameters. The present study is a maiden work consisting of a comprehensive analysis that may be useful in identifying different irregularities and taking corrective measures to converge into a successful experiment. This work relies on the image processing technique which is a fast, simple and effective way to detect defects without going through a long procedure like cutting, etching and optical micrography, analysis and quantification.

2. Materials and Methods

Surface composites (SC) were fabricated to demonstrate how various parameters influence the initial phase irregularities. AA6063 alloy plate having a thickness of 5.0 mm was used as the base material. Plates were perfectly flat and their edges were straight and opposite sides were mutually parallel. FSP was done on a vertical milling machine (Bharat Fritz Werner (BFW), India) (Fig 2(a)) which was specially adapted to perform FSP and the tool head was tilted at an angle of 2°. Parameters such as groove dimensions, tool geometry, plunge depth and reinforcement were altered to produce acceptable quality experiments. A mixture of SiC, iron, Sn and Mn powders in proportion of 60, 28, 5 and 7 (in wt%) respectively was chosen. Sn powder was added as a phase change material (PCM) to control the process temperature and also to act as a distribution facilitator. The low melting point Sn powder is expected to help in better flow of other reinforcement particles (which are loose and discrete) by binding them due to phase change. The phase change also absorbs latent heat and controls the temperature of the material being processed [18-19]. The addition of Fe and SiC powders was made with a view to provide strengthening, resistance to wear and surface hardening. The addition of Mn was made with an objective to study corrosion resistance [20-22]. These properties are expected to be inherited in the present case too. For preparing surface composite, a rectangular slot of dimensions 3 mm (wide) × 2 mm (long) was machined in the middle of the plates in which the reinforcement powder was preplaced. Pin-less tool was used to pack the rectangular slot owing to prevent scattering of powder. Steps for surface composite fabrication are shown in Fig 2(b). The temperature was recorded by installing six K-type thermocouples. These thermocouples were installed nearest at the mid-length of the processed zone (three each at 2.5 mm center-to-center distance on advancing side and retreating side). The thermocouple data was acquired through a specially built data acquisition system and saved in a digital computer. The microstructure and micro-hardness specimens were prepared and polished as per the standard metallographic procedure. Subsequently, the polished specimens were etched with modified poulten reagent. Corrosion test was performed on wonatech potentiostat apparatus in which platinum electrode and saturated calomel electrode are used as the counter and reference electrodes respectively. The samples were exposed to an electrolyte (3.5 wt pct NaCl solution) for 2 hrs.

The irregularities and surface defects of the samples were determined via image processing technique with ImageJ software. Here, the camera-based processing technique was used for detecting surface defects. The image processing steps (shown in Table 1) are as follows:(1) The images of processed area were taken from high resolution digital camera which enabled the acquisition of detailed images of the processed zone; (2) The colored images so obtained were converted to grey scale images with ImageJ software in order to reduce the image data; (3) Adjust the threshold level by intermodes option to create the binary image and reduce noise which was due to the dust and impurity of the processed sample; (4) defects are identified and its shape,

size and orientation were measured shown in Table 3 and analysed by histogram and plot profile options which are shown in Fig 4.

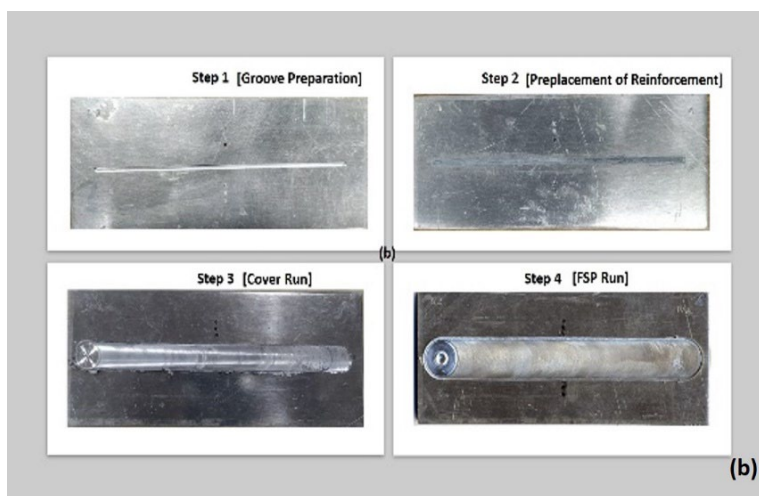
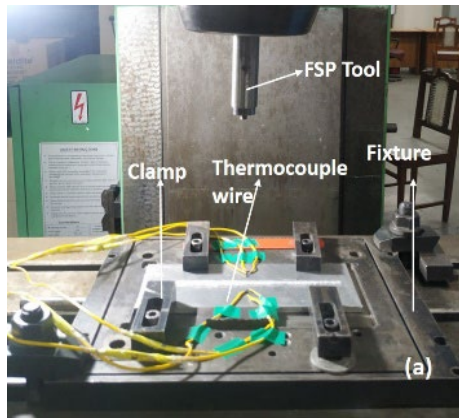


Fig 2. (a) Experimental set-up of FSP; (b) steps for SC fabrication

Table 1 Image processing steps and their respective images of the worst and best run

Variation	Type of Run	Cropped original color images	Grey images	Processed images (ImageJ)
1.	Worst Run			
11.	Best Run			

Table 2 Process parameters window for FSP

Cover Run Parameters						
Shoulder Diameter (mm)	Rotational Speed(rpm)	Traverse Speed (mm/min)	Plunge (mm)			
18	710	16	0.32			
Variation of FSP process Parameters during processing						
Parameter Variation	Shoulder Diameter (mm)	Rotational Speed (rpm)	Traverse Speed (mm/min)	Plunge Depth (mm)	Pin Diameter/Pin length(mm)	Reinforcements (Sn, SiC, Fe, Mn in wt%)
1	20	710	50	4.60	7.5/4.5	5,60,28,7
2	20	710	100	4.60	7.5/4.5	5,60,28,7
3	20	560	160	4.60	7.5/4.5	2,60,31,7
4	20	1120	80	4.60	7.5/4.5	2,60,31,7
5	20	1120	63	4.60	6.5/4.5	2,60,31,7
6	20	900	100	4.60	6.5/4.5	2,60,31,7
7	20	1120	63	4.75	6.5/4.5	2,60,31,7
8	20	1120	63	4.75	6.5/4.5	2,60,31,7
9	20	710	100	4.75	6.5/4.5	2,60,31,7
10	20	1120	100	4.75	6.5/4.5	2,60,31,7
11	20	710	63	4.75	6.5/4.5	2,60,31,7

3. Results and Discussion

3.1 Establishment of range of process parameters

The image processing technique was used to investigate how the change in process parameter affects the FSP pass and to analyse the defects for arriving at successfully processed surface. Table 4 displays actual and processed images of the plates which were friction surface processed. Process parameter window for FSP is shown in Table 2 wherein cover run parameters and variations of FSP process parameter during processing are mentioned separately. Fig V₁₂(a) (V₁₂ means variation 1 in the 1st half plate as well as variation 2 in the other half plate) was obtained by using parameters of variation given in Table 2 after the first trial run and Fig V₁₂(b) represented all the identified surface defects as white blobs. It can be clearly seen that the processed region contains several observable surface defects and irregularities such as scramble, flash, burr and a long rectangular open crater with intermittent closures owing to high amount of PCM and improper process parameter. Fig 3 shows the flowchart for the selection of the range of process parameters, causes of defects and its corrective measures which justifies Table 2. A second pass FSP is commonly applied as a strategy to repair previous pass defects and also to facilitate homogeneous reinforcement distribution [23]. Therefore, here, one would seek the support of literature and apply for a second FSP pass with an objective to close the crater. The details like type of defect and its irregularity in shape, orientation and location provide a lot of information to guide one to change the process parameters.

A close observation of Fig V₃₄ reveals that more scramble is pronounced than in sample S₁, but a triangular crater continues to be observed in the AS. In order to eliminate these defects, the concentration of Sn, which promotes agglomeration, and pin diameter need to be reduced. The reinforcement mixture comprises discrete particles which possess interstitial voids and a larger slot accommodates a greater reinforcement volume and possesses greater interstitial voids. Generally, narrow slot width coupled with adequate slot width (w) to pin diameter (d) ratio should be employed. In the present case, a 3 mm wide slot was processed with a 7.5 mm pin diameter. A large slot width was chosen as it produced a greater volume fraction after processing. During FSP, pin having large diameter empties greater space behind it, which should be replenished by sufficient material being forged due to stirring. For the same shoulder diameter, a pin with large diameter may not generate sufficient forging pressure, keep the emptied space unfilled and the crater would form. The presence of crater suggests that the pin diameter of 7.5 mm is too large for the slot width of 3 mm, resulting in crater formation which should be closed [24,25].

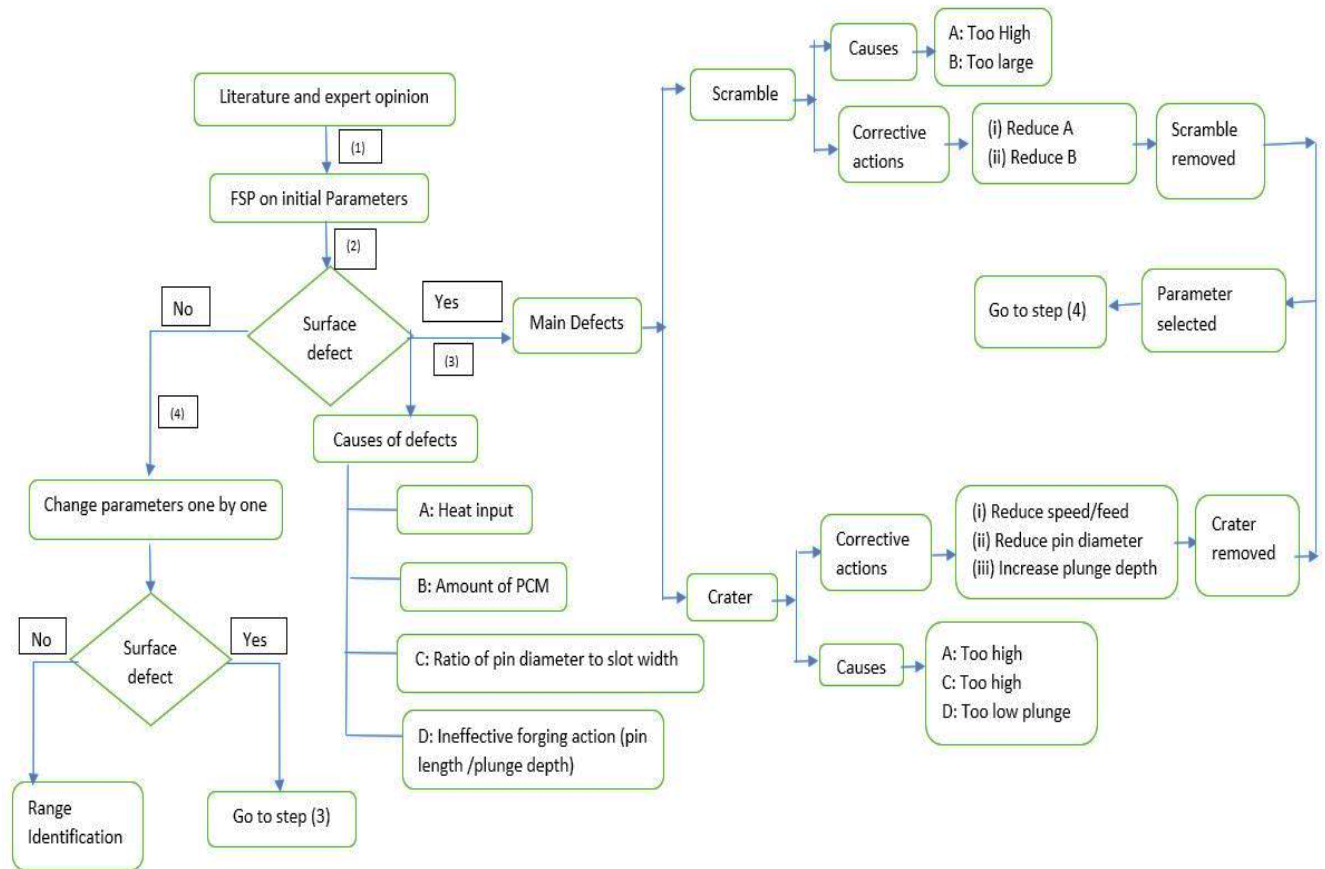


Fig. 3 Flowchart for selection of FSP process parameter

In order to reduce the agglomeration, the concentration of PCM should be reduced; and parameters like **traverse speed should also be reduced to increase the heat input. Reduction in traverse speed means tool engage time during processing per revolution is more.** It is evident from Fig V₅₆ that the scramble was significantly reduced and as the tool progresses it disappeared (as in the region 'a2' of the Figure). However, a rectangular surface crater appears owing to the insufficiency of material which was necessary for consolidation. The third run was performed by taking corrective measures from the previous run as mentioned in Fig 3. The image of the third run shows the irregularities like scramble, crater and flash which are reduced as compared to the second run (refer to Fig V₅₆). But the presence of small defects is still not acceptable. A small amount of flash and a crater could be seen. Flash has been formed because some material was squeezed out of the processed region and insufficient material was left for consolidation and which causes a small crater. The defects were disappeared in the second half part of the run owing to the effect of flash which formed in the beginning disappeared as the FSP progressed. Also, the effect of preheating on the downstream side too resulted in the make-up for the insufficient heat.

In the fourth run, a small amount of flash was found in the beginning owing to high softening that occurred due to high heat. At a high degree of softening, material finds it easy to squeeze out of the shoulder rather than getting forged into the processed zone. The squeezing out of the material in the form of flash causes a material deficiency and makes consolidation difficult, which consequently results in a small rectangular crater as found in plate 4 (Fig V₇₈ 'a1'). **To provide better forging action, the plunge depth was increased from 4.6 mm to 4.75 mm which created a defect free run owing to high heat input and better forging action** (refer to Fig V₇₈ 'a2') [5,11]. Sample V₇₈ reveals that a cleaner and acceptable run can be performed at parameters that administer high heat in the chosen conditions. It is important to expand the parameter range within which clean FSP regions can be created. With this objective variation V₉₁₀ was performed.

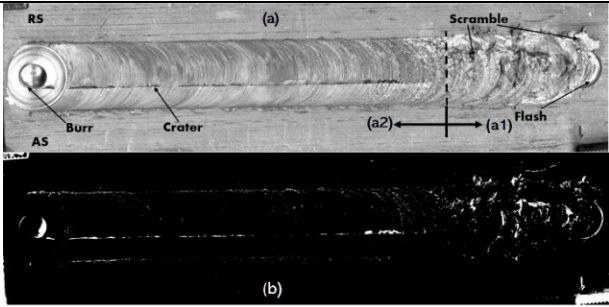
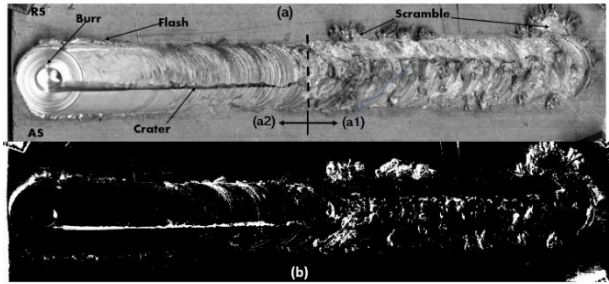
The sample V₉₁₀ shows the run which was performed at two different sets of parameters (refer to Table 2) in the two halves of the plates. It can be observed that no significant defects were produced during the processing. The entire run showed a defect free clean surface of the fabricated SC and thus provided a working range for getting a successful run. **The appearance of the sample confirmed that the rotational speed can be varied between the range of 710 rpm (low heat input)-1120 rpm (high heat input) at a fixed transverse speed i.e. 100 mm/min. Now, instead of increasing rpm whilst keeping speed constant (as in sample V₉₁₀), the transverse speed changes from 100 (low heat input) to 63 (high heat input) mm/min at a fixed rpm of 710 rpm.** The

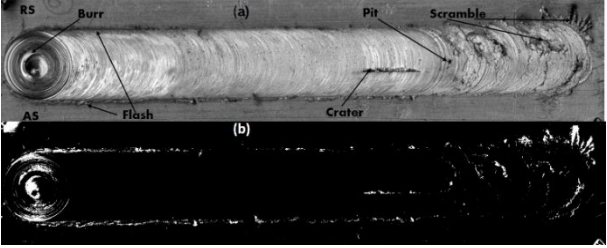
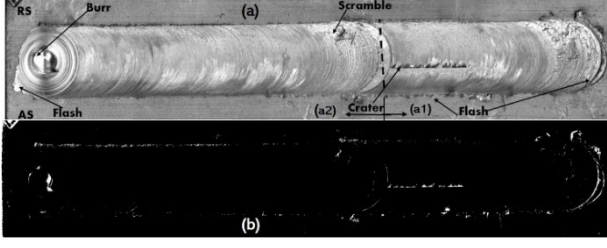
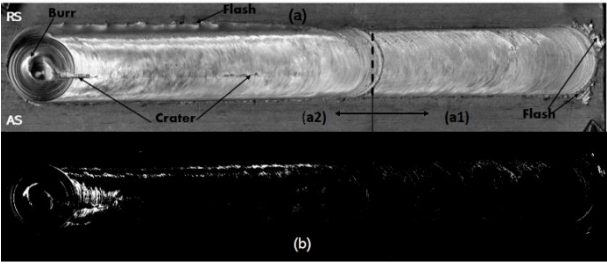
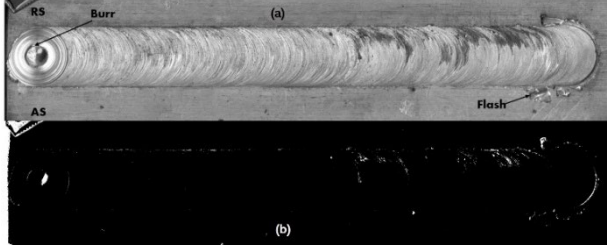
sixth run as in sample V₁₁ was performed at 710 rpm and 63 mm/min (refer to Fig V₁₁) which confirms that this SC run is also free of defects. Thus, a working range of 710 – 1120 rpm and 63 – 100 mm/min speed was established. Table 3 shows the established range of parameter window for FSP wherein fixed parameters and variable process parameters are mentioned for the final run. Taguchi's DoE based L4 orthogonal array was selected from the established range to confirm and validate the window and for optimisation.

Table 3 Established range of parameter window for FSP

Established Range of Parameters				
Fixed Parameters	Shoulder Diameter	Plunge Depth	Pin Diameter/Length	Reinforcement
	20	4.75	6.5/4.5	2,60,31,7 (Sn,SiC,Fe,Mn in wt%)
FSP Process Parameters	Rotational Speed		Traverse Speed	
	710-1120		63-100	
L4 Orthogonal Array				
No. of Experiments	Rotational Speed		Traverse Speed	
1	710		63	
2	1120		100	
3	710		100	
4	1120		63	

Table 4 Scanned and Image processed pictures of all samples (V₁₂-V) along with their descriptions

Variation	Scanned and Image Processed Picture	Description/Visual Observation
Variation 1,2 (V ₁₂)	 <p>Fig. V₁₂</p>	<ol style="list-style-type: none"> 1. Scramble and flash near a1 portion. 2. Two rectangular intermittent craters were found on the advancing side (AS) of size 3.53, 6.807 cm (measured by ImageJ). 3. Small burr at the end of FSP hole opening.
Variation 3,4 (V ₃₄)	 <p>Fig. V₃₄</p>	<ol style="list-style-type: none"> 1. Poor surface and more scrambling defect found in the first half run. 2. In the second half portion 'a2', a triangular crater having a base line of 7 cm near advancing side and whose hypotenuse found near retreating side (RS). 3. Flash on retreating side found.

<p>Variation 5,6 (V₅₆)</p>	 <p>Fig. V₅₆</p>	<ol style="list-style-type: none"> 1. Small sized scramble and a pit found. 2. Small rectangular crater of size 1.57cm near advancing side. 3. Flash and burr at the end of the run.
<p>Variation 7,8 (V₇₈)</p>	 <p>Fig. V₇₈</p>	<ol style="list-style-type: none"> 1. Small amount of flash found in the first half (portion 'a1'). 2. Small rectangular crater of size 2.197cm was found near the advancing side. 3. In the second half of 'a2' portion small scramble was found at the beginning of the run. 4. Small burr and flash at the end of the run
<p>Variation9,10 (V₉₁₀)</p>	 <p>Fig. V₉₁₀</p>	<ol style="list-style-type: none"> 1. Small flash obtained at the beginning on 1st half portion of 'a1'. 2. Two small rectangular craters of size 1.1cm each were found near the advancing side. 3. Large amount of flash in the retreating side.
<p>Variation 11 (V₀₁₁)</p>	 <p>Fig. V₀₁₁</p>	<ol style="list-style-type: none"> 1.No defect was found in the processed region.

Gray level distribution of V₉₁₀ is showing a large variation of grayscale intensities along the processed zone in Fig 4. Abrupt crests and troughs in the range of 10-30 were the indications of the discontinuity and inconsistency of the processed zone i.e. presence of defect. A small variation in the range of 1-5 was observed in V₁₁ which signified that the processed zone was having defect free surface. The histogram of the gray level image shows the distribution of intensities in the range 0-255 and is used to reveal the information related to the irregularities in the processed zone. In V₀₁₁, the histogram does not have any pixel below the gray level number of 70 which signifies the defect free processed zone. Whereas in V₁₂, this value is below 20 which means the processed zone is having defects [26,27].

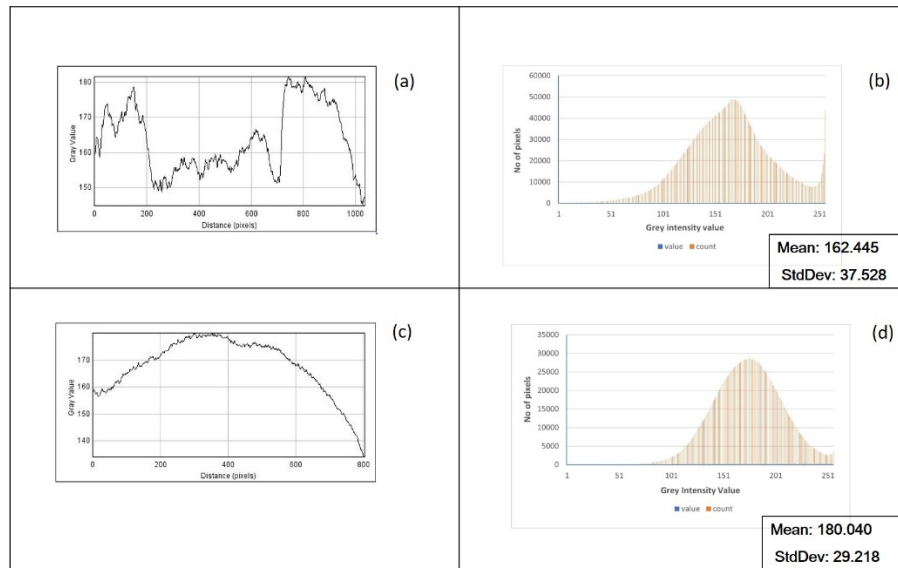


Fig. 4 (a,c) grey level distribution; **(b,d)** histogram of gray images for V_{12} and V_{011} respectively

3.2 Study of ripple formation

The surface of the processed surface, as obtained after FSP, also has a typical surface morphology which can be useful in many analyses. The surface appearance of the region processed by FSP (Fig 5) shows a regular circular ripple pattern which may be correlated to the action of the shoulder during the advancement of the tool. The formation mechanism of such surface patterns is relevant to the tool features (such as features in the shoulder etc.) and flow interaction (due to the presence of feature on the pin e.g. presence of flute, nature of threads etc.) underneath the shoulder. These regular pitch ripples are produced by the final ejection of the layers of depositing mass at the trailing circumferential edge of the shoulder, during the traverse of the tool. As the rotational direction of the shoulder changes from RS to AS, at this moment the materials in the AS are mixed and appear like a ripple line because of the increase in the flow force at the AS. The actual size of the ripples can be defined as the ratio of the traverse speed of the workpiece to the rotation speed of the tool. Table 5 shows the theoretical and actual measured distance (by ImageJ) between the ripples [28,29].

Table 5 Distance between the ripple at different process parameter

No.	Rotational Speed(rpm)	Traverse Speed(mm/min)	Distance of the Ripple (mm) (By imageJ)	Distance per revolution of tool(mm)
a (Variation 9)	710	100	0.142	0.1408
b (Variation 10)	1120	100	0.088	0.089

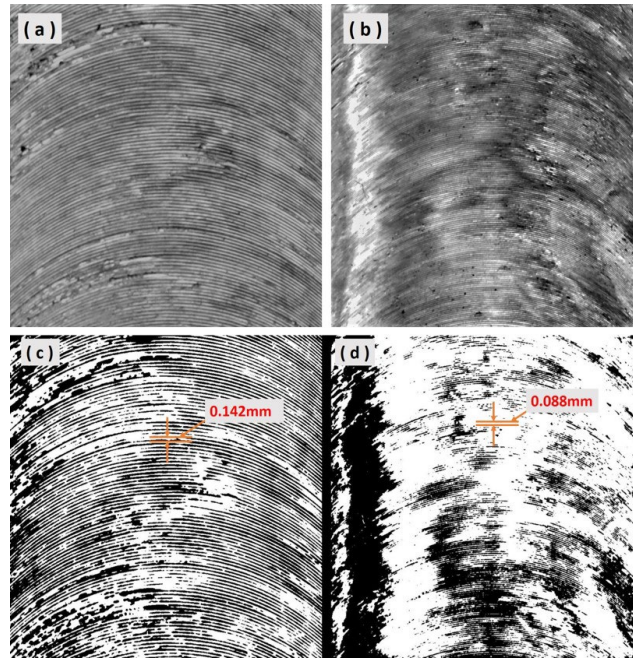


Fig. 5 (a,b):Ripple formation at different processing parameters; (c,d): image analysis of the ripple

3.3 Confirmation of established range

Experiment no.1 from L4 orthogonal array is conducted for further confirmation of the established range. Thermal, microstructural, micro-hardness, and corrosion analyses have been done. The processed plate after FSP i.e new Friction stirred processed plate (NFP) is shown in Fig 6 where locations of thermocouple are clearly mentioned for temperature measurements. The results are discussed in the following sections.

3.3.1 Thermal Analysis

Fig 7 (a) depicts the main effects plot for Signal to noise (S/N ratios) which were calculated for each experiment in L4 OA. Lower values of peak temperature was chosen as desired and therefore smaller-the-better characteristic were used to calculate the S/N ratio. Fig 7(b) shows time-temperature profile of achieved optimum parameter which depicted that the thermocouple output for the entire duration of the FSP run. It is noticeable that the highest temperature i.e. 423.25°C occurred on AS because more heat of deformation is generated during beginning of processing from this side. Initially, the temperature has increased slowly because of preheating of the sample and after that curve rises more and steeper owing to the FSP tool acting as a moving heat source. The temperature reached to its peak value when the tool passed through the thermocouple location. The temperature plot beyond the thermocouple location drops gradually indicating a gradual cooling.

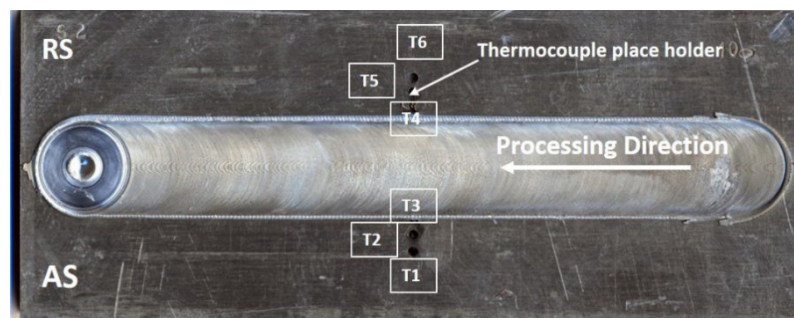


Fig. 6 Location of thermocouple for thermal analysis in NFP

Further to notice that the peak temperature outputs of the thermocouples which are located farther from the processing-line centre drop sharper than those located nearer to the processing line.

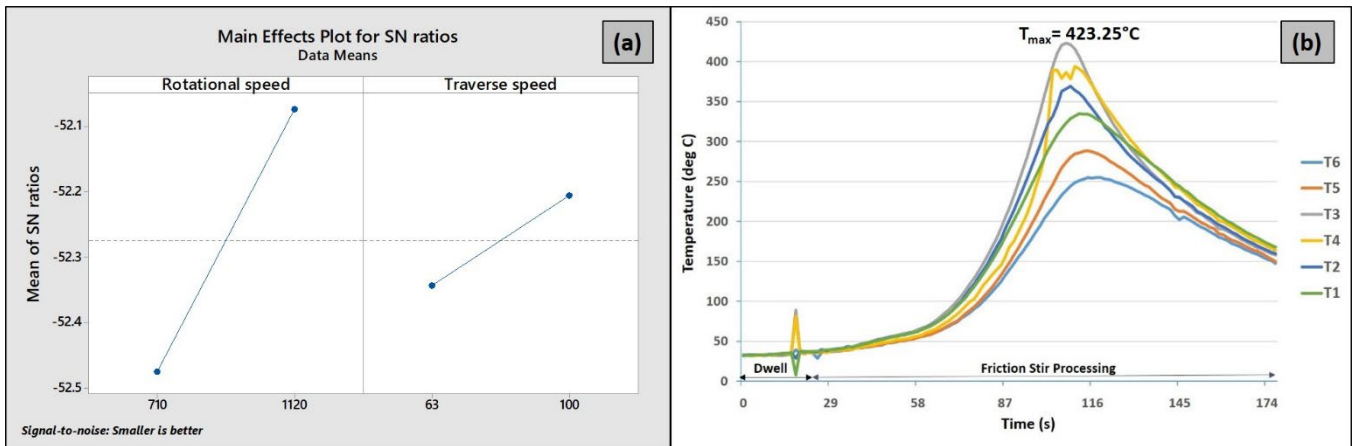


Fig. 7(a): Main effects plot for SN ratios, (b): Temperature vs Time plot of NFP

3.3.2 Microstructural and Micro-hardness Measurements

Fig 8 depicts the macrograph of the processed region in NFP. Basin-shaped macrograph showed a broad opening at the upper portion owing to high frictional heat and deformation by contact between the shoulder and processed surface. The microstructure of base material and SZ of NFP are shown in Fig 10 where grains are clearly visible. Base material has coarse grains whereas fine, equiaxed and uniformly distributed grains are present in SZ owing to dynamic recrystallization (fig10 (c)).

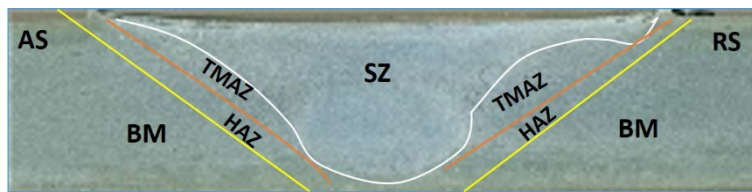


Fig.8 Macrostructure of the processed zone

SEM examination was performed on NFP to understand the distribution of reinforcement particles in the stir zone (SZ) shown in Fig 9. Distribution of reinforcement is more even and homogeneous due to proper mixing with the matrix. This is attributed due to processing at desired process parameters.

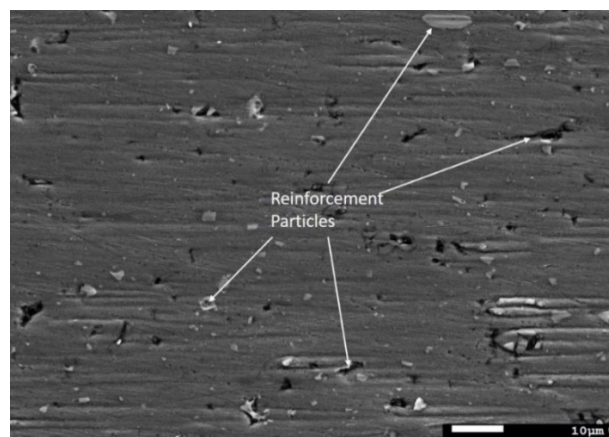


Fig. 9 SEM image of the processed zone

Moreover, micro-hardness test is performed on the base material (BM) as well as on NFP from AS to RS. Hardness value of base material (BM) as well as SZ of NFP are 65.03 Hv and 90.69 Hv respectively. Higher hardness values are attributed due to grain refinement and Orowan strengthening during the friction stir processing.

3.3.3 Corrosion Analysis

Similarly corrosion study is carried out on the base material as well as on the NFP to study the electrochemical behavior of the samples. Fig 10 shows the microstructure of the base material and SZ of the NFP before and after corrosion. Corroded patches are more visible in base material in comparison to the SZ. This is due to the fact corrosion rate and grain boundaries are dependent on each other. **With increase in the homogeneity of microstructure the grain boundary serves as the barrier owing to the shift in positive corrosion potential, reduced corrosion current density** which resists the corrosion process [30, 31]. Fig 11 depicts the potentiodynamic polarization curve i.e Tafel plot for the base material and NFP.

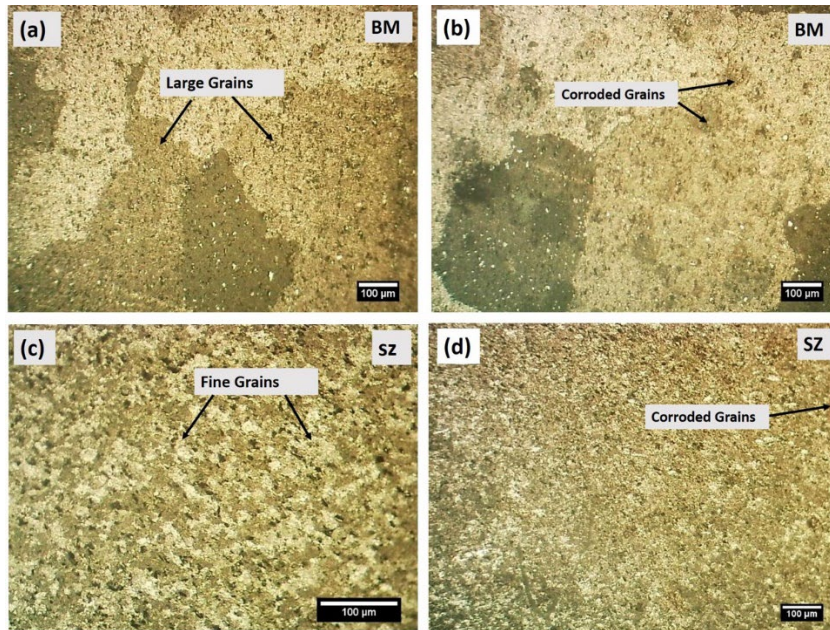


Fig. 10 Microstructure of (a) base material before corrosion (b) base material after corrosion (c) SZ of NFP before corrosion (d) SZ of NFP after corrosion

Higher corrosion potential (E_{corr}) is higher and lower corrosion current density (J_{corr}) are obtained in the base material as compared to the NFP shown in Fig 11. As higher values of J_{corr} represents the higher corrosion rate therefore, the base material shows the lower corrosion resistance compared to the NFP [32]. SZ of the NFP shows higher corrosion resistance because of the reinforcement elements and fine grain size. Table 6 shows the values of corrosion potential (E_{corr}), corrosion current density (J_{corr}) and corrosion rate (CR-mpy).

Table 6 Corrosion test results of base material and NFP

Specimens	E_{corr} (V)	J_{corr} (A/cm ²)	CR-mpy
Base material	-0.774787	6.911955E-7	0.310931
NFP	-0.8909	5.969871E-7	0.268552

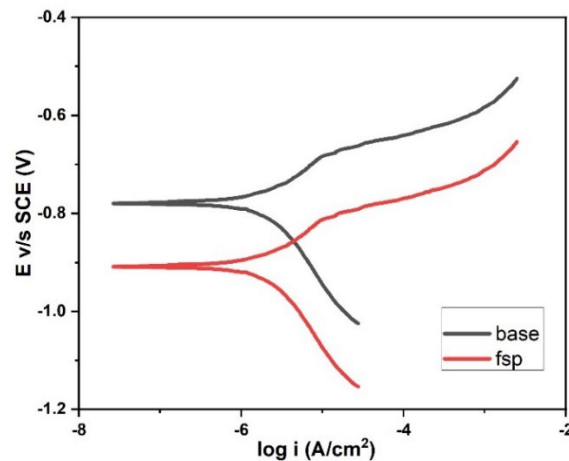


Fig. 11 Potentiodynamic polarization curves of the BM and NFP

4. Conclusions

In this research work, an attempt to establish a working range of surface composites that were fabricated on AA6063 alloy by FSP. The surface defects that occurred during FSP have been classified into scramble, crater, flash and burr. The important results of the present study are mentioned below:

1. Scramble defect is formed due to the low heat input and agglomeration of Sn particles which are added to the reinforcement as phase-change-material. It was found that a higher concentration of Sn causes agglomeration which produces scramble. The Sn powder is added in the reinforcement to control the process temperature and also as a distribution facilitator.
2. It was found that a ratio of slot width (w) to pin diameter (d) equal to 0.49 could eliminate the crater defect effectively.
3. It was found that the parameters which result in either too high or too low heat may lead to defect formation. The processing parameter combination may lead to either insufficient or excessive heat input and may affect material movement and consolidation that deteriorate the surface morphology of the processed region.
4. Parameters leading to too high heat input lead to excessive softening and result in the expulsion of material out of the shoulder in the form of flash. Parameters causing less heat input cause lack of material consolidation which results in scramble.
5. Maximum temperature is achieved at AS because more heat of deformation is generated during the beginning of processing from this side.
6. Microscopic and SEM image were taken from the extreme processing conditions i.e NFP reveals the homogenous particle distribution which verifies that the established range can provide a feasible process parameter window in very few experimental runs.
7. Hardness of NFP is increased by 28.29% as compared to base material because of fine grains and homogenous distribution of the reinforcement particles.
8. NFP has higher corrosion resistance compared to the base material owing to **the increase in the homogeneity of microstructure wherein grain boundary serves as the barrier** that resists the corrosion process.

Acknowledgment

The authors extend their appreciation to the Deanship of Scientific Research at King Saud University.

References

1. Mishra, R. S., & Ma, Z. Y. (2005). Friction stir welding and processing. *Materials science and engineering: R: reports*, 50(1-2), 1-78.
2. Gangil, N., Maheshwari, S., Nasr, E. A., El-Tamimi, A. M., El-Meligy, M. A., & Siddiquee, A. N. (2018). Another approach to characterize particle distribution during surface composite fabrication using friction stir processing. *Metals*, 8(8), 568

3. Bharti, S., Ghetiya, N. D., & Patel, K. M. (2021). A review on manufacturing the surface composites by friction stir processing. *Materials and Manufacturing Processes*, 36(2), 135-170.
4. Heidarzadeh, A., Mironov, S., Kaibyshev, R., Çam, G., Simar, A., Gerlich, A., ... & Withers, P. J. (2021). Friction stir welding/processing of metals and alloys: A comprehensive review on microstructural evolution. *Progress in Materials Science*, 117, 100752..
5. Dialami, N., Cervera, M., & Chiumenti, M. (2020). Defect formation and material flow in Friction Stir Welding. *European Journal of Mechanics-A/Solids*, 80, 103912
6. Wang, Z. Z., & Zhang, Y. M. (2007). Image processing algorithm for automated monitoring of metal transfer in double-electrode GMAW. *Measurement Science and Technology*, 18(7), 2048
7. Ranjan, R., Khan, A. R., Parikh, C., Jain, R., Mahto, R. P., Pal, S., ... & Chakravarty, D. (2016). Classification and identification of surface defects in friction stir welding: An image processing approach. *Journal of Manufacturing Processes*, 22, 237-253.
8. Rajakumar, S., Muralidharan, C., & Balasubramanian, V. (2010). Optimization of the friction-stir-welding process and tool parameters to attain a maximum tensile strength of AA7075-T6 aluminium alloy. *Proceedings of the Institution of Mechanical Engineers, Part B: Journal of Engineering Manufacture*, 224(8), 1175-1191.
9. Kim, Y. G., Fujii, H., Tsumura, T., Komazaki, T., & Nakata, K. (2006). Three defect types in friction stir welding of aluminum die casting alloy. *Materials Science and Engineering: A*, 415(1-2), 250-254.
10. Khan, N. Z., Siddiquee, A. N., Al-Ahmari, A. M., & Abidi, M. H. (2017). Analysis of defects in clean fabrication process of friction stir welding. *Transactions of nonferrous metals society of china*, 27(7), 1507-1516
11. Kah, P., Rajan, R., Martikainen, J., & Suoranta, R. (2015). Investigation of weld defects in friction-stir welding and fusion welding of aluminium alloys. *International Journal of Mechanical and Materials Engineering*, 10(1), 26.
12. Bayazid, S. M., Farhangi, H., & Ghahramani, A. (2015). Effect of pin profile on defects of Friction Stir Welded 7075 Aluminum alloy. *Procedia materials science*, 11, 12-16
13. Li, B., Shen, Y., & Hu, W. (2011). The study on defects in aluminum 2219-T6 thick butt friction stir welds with the application of multiple non-destructive testing methods. *Materials & Design*, 32(4), 2073-2084.
14. Arbegast, W. J., Coletta, E. R., & Li, Z. (2001, February). Characterization of friction stir weld defect types. In *TMS 2001 Annual Spring Meeting*, New Orleans, LA (pp. 11-15).
15. Zhou, N., Song, D., Qi, W., Li, X., Zou, J., & Attallah, M. M. (2018). Influence of the kissing bond on the mechanical properties and fracture behaviour of AA5083-H112 friction stir welds. *Materials Science and Engineering: A*, 719, 12-20.
16. Kah, P., Rajan, R., Martikainen, J., & Suoranta, R. (2015). Investigation of weld defects in friction-stir welding and fusion welding of aluminium alloys. *International Journal of Mechanical and Materials Engineering*, 10(1), 26.
17. Mohan, A., & Poobal, S. (2018). Crack detection using image processing: A critical review and analysis. *Alexandria Engineering Journal*, 57(2), 787-798.
18. Confalonieri, C., Grimaldi, A. T., & Gariboldi, E. (2020). Ball-milled Al-Sn alloy as composite Phase Change Material. *Materials Today Energy*, 100456
19. Gangil, N., Maheshwari, S., & Siddiquee, A. N. (2018). Novel Use of Distribution Facilitators and Time-Temperature Range for Strengthening in Surface Composites on AA7050-T7451. *Metallography, Microstructure, and Analysis*, 7(5), 561-577.
20. Najafi, A., Movahedi, M., & Yarandi, A. S. (2018). Properties-microstructure relationship in Al-Fe in situ composite produced by friction stir processing. *Proceedings of the Institution of Mechanical Engineers, Part L: Journal of Materials: Design and Applications*, 1464420718803752
21. Jain, V. K. S., & Muthukumar, S. (2019). Influence of SiC content on microstructure and tribological properties of friction stir-processed SiC/AA5083 surface composites. *Metallurgical and Materials Transactions A*, 50(6), 2933-2944 .
22. Xiaoyan, L., Mingzhao, L., Liuqun, F., Haiyan, W., Chong, F., & Hua, M. (2014). Effects of Mn on corrosion resistant property of AZ91 alloys. *Rare Metal Materials and Engineering*, 43(2), 278-282.
23. Mehdi, H., & Mishra, R. S. (2021). Consequence of reinforced SiC particles on microstructural and mechanical properties of AA6061 surface composites by multi-pass FSP. *Journal of Adhesion Science and Technology*, 1-20.
24. Bourkhani, R. D., Eivani, A. R., Nateghi, H. R., & Jafarian, H. R. (2020). Effects of pin diameter and number of cycles on microstructure and tensile properties of friction stir fabricated AA1050-Al2O3 nanocomposite. *Journal of Materials Research and Technology*.
25. Gangil, N., Maheshwari, S., & Siddiquee, A. N. (2018). Multipass FSP on AA6063-T6 Al: Strategy to fabricate surface composites. *Materials and Manufacturing Processes*, 33(7), 805-811.

26. Sinha, P., Muthukumaran, S., Sivakumar, R., & Mukherjee, S. K. (2008). Condition monitoring of first mode of metal transfer in friction stir welding by image processing techniques. *The International Journal of Advanced Manufacturing Technology*, 36(5-6), 484-489.
27. Murthy, V., Ullegaddi, K., Mahesh, B., & Rajaprakash, B. M. (2017). Application of image processing and acoustic emission technique in monitoring of friction stir welding process. *Materials Today: Proceedings*, 4(8), 9186-9195.
28. Tamadon, A., Pons, D. J., & Clucas, D. (2020). Structural anatomy of tunnel void defect in bobbin friction stir welding, elucidated by the analogue modeling. *Applied System Innovation*, 3(1), 2
29. Yoon, T. J., & Kang, C. Y. (2015). Observations on metallurgical phenomena and formation of onion ring nugget during friction stir lap welding of dissimilar aluminum by a new 3D technique. *Materials Letters*, 142, 253-257.
30. Majeed, T., Mehta, Y., & Siddiquee, A. N. (2021). Precipitation-dependent corrosion analysis of heat treatable aluminum alloys via friction stir welding, a review. *Proceedings of the Institution of Mechanical Engineers, Part C: Journal of Mechanical Engineering Science*, 235(24), 7600-7626.
31. Nam, N. D., Dai, L. T., Mathesh, M., Bian, M. Z., & Thu, V. T. H. (2016). Role of friction stir welding–traveling speed in enhancing the corrosion resistance of aluminum alloy. *Materials Chemistry and Physics*, 173, 7-11.
32. Mahesh, V. P., Gumaste, A., Meena, N., Alphonsa, J., & Arora, A. (2020). Corrosion behavior of aluminum surface composites with metallic, ceramic, and hybrid reinforcements using friction stir processing. *Metallurgical and Materials Transactions B*, 51(5), 2131-2146.